Hindawi
Advances in Condensed Matter Physics
Volume 2023, Article ID 8706698, 13 pages
https://doi.org/10.1155/2023/8706698

Research Article

Degradation of Metronidazole from Aqueous Environment Using Hydrothermally Synthesized ZnO, N-Doped ZnO, and ZnO/AC Nanoparticles

Masuma Bagum,[1] Shariful Islam ,[1] Easir Arafat Khan,[2] Jahirul Islam Khandaker,[1] and Farid Ahmed[1]

[1]*Department of Physics, Jahangirnagar University, Savar, Dhaka 1342, Bangladesh*
[2]*Department of Chemical Engineering, Bangladesh University of Engineering & Technology, Dhaka, Bangladesh*

Correspondence should be addressed to Shariful Islam; s_islam@juniv.edu

Received 18 April 2023; Revised 28 May 2023; Accepted 2 June 2023; Published 28 June 2023

Academic Editor: Tholkappiyan Ramachandran

ZnO, ZnO (calcined at 400°C), nitrogen-doped ZnO nanoparticles, and activated carbon (AC) impregnated with ZnO (ZnO/AC) nanocomposites were synthesized by the hydrothermal method. The structural, morphological, and optical properties of the synthesized complexes were studied by X-ray diffraction (XRD), energy dispersive X-ray spectroscopy (EDS), scanning electron microscopy (SEM), transmission electron microscopy (TEM), Fourier transformation infrared analysis (FTIR), Brunauer–Emmett–Teller (BET) analysis, and UV-visible spectroscopy analysis. The degradation of the antibiotic metronidazole (MNZ) from aqueous solutions was examined by the photocatalytic process of those synthesized complexes. Among the four complexes, ZnO/AC was confirmed to be a capable prospective both as an efficient photocatalyst and as an adsorbent. The optimal photodegradation condition obtained was 0.9 g/L and pH = 9. After 300 minutes, 99% of MNZ was removed by ZnO/AC. Finally, gas chromatography-mass spectroscopy was conducted to identify the degradation intermediates.

1. Introduction

Bacteria are the source of disease as they eject toxins (e.g., botulism) [1, 2] which are at large when the bacteria are split (e.g., typhoid) [3], or the sensitivity is increased to their antigenic properties (e.g., tuberculosis) [4]. An antibiotic is an antibacterial agent that is widely active in hostile bacterial infections for either killing or inhibiting their growth [5]. The most common antibiotics that have been used in healthcare are penicillin, metronidazole, streptomycin, chloramphenicol, chlortetracycline, neomycin, azithromycin, and ciprofloxacin [6]. The antibiotics which are not used or are metabolized end up in land, drains, surface water, or toilets [7]. When bacteria adapt to these antibiotics (which are designed to treat bacterial infections), antibiotic resistance develops. Therefore, antibiotics may not work properly in the human body [8, 9]. There is still no comprehensive way out for stopping environmental pollution with these antibiotic elements [10]. Antibiotic and their metabolites were quantified in the concentration of nanogram to milligram per liter from the aquatic environments of Poland, Europe [10], the United States [11], Bangladesh [12], and even Antarctic seawater [13] by separate study which is alarming for living organism such as human[14], animal [15], agriculture [16]. Among the antibiotics, some antibiotics such as penicillin are easily degradable, but most of them do not degrade naturally [17]. Metronidazole ($C_6H_9N_3O_3$) (MNZ) which belongs to the nitroimidazole antibiotic group has a solubility of about 9.5 g/L in water and a molecular weight of 171.2 g/mol [18]. In majority of the

time, it is employed to treat infectious disorders brought about by hostile bacteria and protozoa [6]. MNZ is easily accumulated in aqueous surroundings because it is very much soluble in water and are nonbiodegradable [19]. Thus, an effective method to eliminate MNZ is required.

Several approaches, including ultraviolet (UV) filtration [20], electrochemical degradation process [21], catalytic ozonation process [22], Sono–Fenton process [23], and photocatalytic degradation under UV and visible radiation with different composites, were reported to reduce the amount of MNZ present in drinkable and waste water from industries.

The photocatalytic degradation under UV and visible radiation was conducted with various nanoparticles such as TiO_2 [24], ZnO [24], ZnO stabilized in stone surface [25], LP-ZnO stabilized by lemon peel aqueous extract [26], Ag-ZnO [19], CuO [27], Fe(OH)3 [28], and FeNi3/SiO2/CuS magnetic [29] nanocomposite, and many more were conducted. The photocatalytic reactions are represented by the following equations [16, 18]:

$$
\begin{aligned}
&ZnO + h\gamma \longrightarrow e^- + h^+ \\
&e^- + O_2 \longrightarrow \bullet O_2^- \\
&h^+ + H_2O \longrightarrow H^+ + \bullet OH \\
&h^+ + \bullet OH^- \longrightarrow \bullet OH \\
&\frac{OH}{\bullet O_2^-} + \text{organic chemicals} \longrightarrow \text{final products}\,(CO_2, H_2O, \text{etc})
\end{aligned}
\tag{1}
$$

Zinc oxide (ZnO) is the most widely used photocatalyst due to its stability, affordability, and lack of toxicity. Pure ZnO has a band gap energy of about 3.28 eV, which is 2.9 eV for a nitrogen-doped ZnO catalyst [30]. The band gap of the specimens decreased when the Nd/Gd doping content ratio grew into ZnO according to the UV-vis data [31].

ZnO is usually used in wastewater management in the form of nanoparticles since it has an extremely huge surface area compared to its volume. Moreover, for centuries, activated carbon has been used as an excellent adsorption substrate because it has a high BET surface area and micropore volume. M. Sivachidambaram et al. showed the preparation of activated carbon (specific surface area 633.43 m^2/g) from borassus flabellifer flower under different activation temperatures by a chemical activation method applied as a precursor material for the production of low cost-high performance activated carbon electrode materials for electric double layer capacitors [32]. Yee et al. provided a roadmap for producing high-quality supercapacitors using carbon-based electrodes [33]. Shamima Begum and Ahmaruzzaman studied the synthesis of SnO_2/activated carbon (from the stem of Corchorus olitorius) nanocomposites by the hydrothermal method that showed an invincible photocatalytic property in the degradation of naproxen (NPX) under direct sunlight [34]. Tran Thi and Lee fabricated composite materials of activated carbon fiber (ACF) coated with zinc oxide (ZnO) using a commercial microwave oven which exhibited removal capacity (over 99%) and mineralization (90.7%) of tetracycline in aqueous solution within 1 h under UV irradiation [35]. Accordingly, it is found that metal oxide-fabricated AC exhibits a synergistic impact of AC on adsorption and metal oxide on the photodegradation of dangerous pollutants.

The objective of this study is to the synthesize, evaluate, and compare the following: ZnO, ZnO (calcinated at 400°C), nitrogen-doped ZnO (N-ZnO), and activated carbon impregnated with ZnO (ZnO/AC) nanocomposites by the hydrothermal method, for their potentiality for metronidazole removal from wastewater.

2. Materials and Methods

2.1. Chemicals. Zinc acetate dihydrate $Zn(CH_3COO)_2{\cdot}2H_2O$, sodium hydroxide NaOH, ethanol C_2H_5OH, orthophosphoric acid (H_3PO_4), and urea $(NH_2)_2CO$ were used.

2.2. Synthesis

2.2.1. Synthesis of ZnO Nanoparticles. The reference solution **A** was made by combining 25.0 mL of deionized water with 10.00 g of NaOH and 5.48 g of $Zn(CH_3COO)_2.2H_2O$. 66 mL of ethanol and 6 mL of reference solution A were combined in a beaker while being constantly stirred. This was ultrasonicated for 10 minutes and immediately transferred to a Teflon-lined autoclave with 100 ml capacity. Then, it was placed in a furnace and the temperature was increased to 150°C and it was maintained there for 13 hours. The autoclave was then given time to cool down to an ambient temperature. The resulting sediment was thoroughly cleaned using distilled water and ethanol before being dried at 60°C.

2.2.2. Synthesis of ZnO (400°C) Nanoparticles and ZnO (400°C). ZnO (400°C) was prepared by calcining ZnO at 400°C for 4 hr and slowly cooled down.

2.2.3. Synthesis of N-ZnO Nanoparticles. 66 mL of ethanol and 6 mL of reference solution A were combined in a beaker while being constantly stirred. After stirring for an hour, 200 mg of urea was obtained. This was ultrasonicated and collected in a Teflon-lined autoclave with a 100 ml capacity. In a furnace, the autoclave's temperature was increased to 150°C and it was maintained there for 13 hours. The autoclave was then given time to cool down to ambient temperature. The resulting sediment was thoroughly cleaned using distilled water and ethanol before being dried at 60°C.

2.2.4. Synthesis of ZnO/AC Nanocomposites. Stems of the neem plant (Azadirachta indica) were gathered from the adjacent city of Dhaka and chemically activated to create activated carbon (AC). Neem stems were carefully chopped into pieces of a few centimetres, cleaned with distilled water,

and dried in a furnace for 24 hours at 100°C. Then, 120 g of these neem pieces were placed in a muffle furnace and heated to 500°C at a rate 1°Cs^{-1} for 4.5 hours and cooled down. The ashes were washed away, and only coals were taken. Then, these were grinded/crushed into powder using a Panasonic home blander, and this was named as PCC (precarbonised carbon). The weight ratio for neem before drying, after drying, and PCC is 10 : 5 : 1; that is, approximately 12 g of PCC is obtained from 120 g of neem stem. 5 g of PCC were impregnated with orthophosphoric acid (H_3PO_4) solution (20 mL H_3PO_4 + 5 mL DW) and heated on a hot plate for 4 hours with continuous stirring at 110°C for even distribution. For 2 hours, the mixture was heated to 700°C in a furnace. This was crushed and repeatedly cleaned with distilled water until the pH was neutral. The product was then dried for an entire night at 120°C before being grinded into tiny homogeneous particles with a mortar and pestle.

Again, 66 mL of pure alcohol, 6 mL of reference solution A, and 1.365 g of AC were combined in a beaker and continuously stirred for 30 minutes before being ultrasonicated for 10 minutes. This was collected in a Teflon-lined autoclave that was heated to 150°C and maintained at that temperature for 24 hours in a furnace. The autoclave was then cooled down to an ambient temperature. The resulting sediment was thoroughly cleaned using distilled water and ethanol before being dried at 60°C to produce ZnO/AC.

2.3. Characterization Instruments. Carbon-coated samples were used for SEM and EDS studies, and the ZEISS EVO 18 Research SEM equipment was used to monitor them. For IR analysis, the IRPrestige-21 spectrometer was used. The synthesized materials underwent XRD analysis by using a GNR Explorer diffractometer from $2\theta = 20°$–$70°$ with a scanning step of 0.01°. UV-vis spectroscopy was conducted using a HITACHI UH4150 UV-vis system. BET Sortometer (BET-201-A) was used to measure the surface area per unit volume. Talos f200x was used for TEM. UT 383 mini Light Meter was used to measure the light intensity of UV light at the surface of MNZ solution under degradation.

2.4. Metronidazole Removal Reactor Setup and Reaction Analysis. The mixture of photocatalysts and MNZ solution was kept under three UV lights that emit radiation at 254 nm wavelength in an open 200 mL hemispherical stainless glass vessel. The UV lamps were placed at a distance of 12 cm from the surface of the solution where the effective power was about 20 W. This reaction container was covered with a transparent glass plate to avoid evaporation of metronidazole solution under continuous stirring (250 rpm). In each experiment, various known amounts of photocatalysts were suspended in 40 mL of model metronidazole aqueous solution of 80 mg/L concentration. Before illuminating the lamps, the solution was initially mixed in the dark for 30 minutes to allow for adsorption. After starting the UV light irradiation, 1.5 mL of samples were taken and placed into a collection tube at predetermined intervals. These underwent a 10-minute centrifugation at 1300 rpm while having been passed through 0.45 microns nylon 6,6 membranes. The amount of MNZ in the solution was then measured by using a UV-vis spectrophotometer with a maximum absorption wavelength of 320 nm. Each experiment was carried out in identical conditions, and they were performed twice to make an average.

The analysis of the kinetics of degradation was carried out according to the Langmuir–Hinshelwood model [19]. The model is represented as

$$r = -\frac{dC}{dt} = k\theta_s = \frac{kK_LC}{1 + K_LC}. \quad (2)$$

This model relates the degradation rate r (mg·L^{-1}min^{-1}) and the fractional surface coverage of the catalyst (θ_s) where C is the concentration of MNZ (mg·L^{-1}), t is the reaction time (min), k is the rate constant (mg·L^{-1} min^{-1}), and K_L is the Langmuir adsorption constant (L·mg^{-1}). Under the conditions of relatively low MNZ concentrations and/or weak adsorption, K_LC will be much smaller than 1.

Therefore, the abovementioned equation is represented as

$$\frac{dC}{dt} = -kK_LC = -k_{app}C, \quad (3)$$

where k_{app} denotes the apparent first-order rate constant. By integrating the abovementioned equation, it can be written as

$$\ln\left(\frac{C}{C_0}\right) = -K_{app}t, \quad (4)$$

where C_0 is the initial concentration of MNZ. The K_{app} value is obtained from the slope of the plot of $\ln(C_0/C)$ vs. t.

3. Results and Discussion

3.1. Structural and Morphological Characterization

3.1.1. XRD Analysis. Figure 1 shows the XRD patterns of ZnO, ZnO (calcined at 400°C), N-doped ZnO, and ZnO doped on activated carbon. The diffraction peaks of pure ZnO are observed at 2θ values of 31.74°, 34.41°, 36.14°, 47.55°, 56.56°, 62.91°, 66.35°, 68°, and 69.14° corresponding to the planes of (100), (002), (101), (102), (110), (103), (200), (112), and (201), respectively, which matches the previous report. No peak for impurity was observed. All the peaks obtained for ZnO, ZnO (400°C), and N-ZnO are assigned to the standard hexagonal wurtzite ZnO crystal structure (COD 96–901–1663). The peaks obtained for ZnO/AC are assigned to the standard hexagonal wurtzite ZnO crystal structure (COD 96–210–7060).

The lattice parameters are shown in Table 1. The lengths of a and b are the same, while that of c is different in all the samples. Besides, the lattice parameters of all the samples are almost the same and hence also the cell volume. Among the samples, the cell volume of ZnO/AC is the smallest.

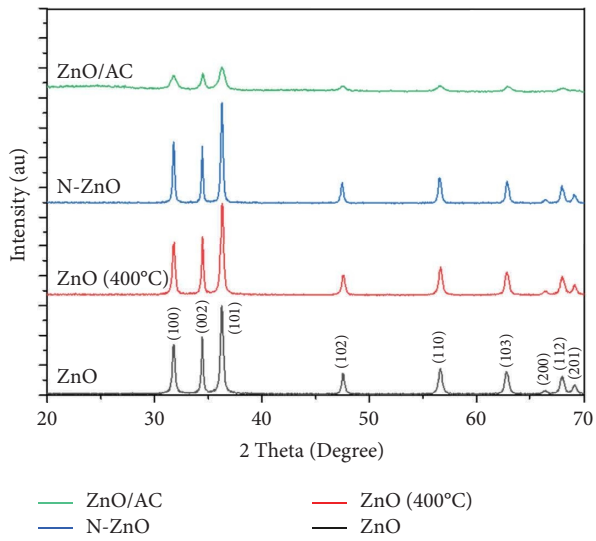

Figure 1: XRD spectra of synthesized complexes.

Table 1: Lattice parameters of the samples.

Samples	Lattice parameters Å parameters (Å)		Volume $(Å)^3$
	$a = b$	C	
ZnO	3.2490	5.2070	47.601
ZnO (400°C)	3.2490	5.2070	47.601
ZnO/AC	3.2417	5.1876	47.211
N-ZnO	3.2490	5.2072	47.603

The average crystallite size was calculated by the Debye–Scherrer equation [36] written as follows:

$$D = \frac{k\lambda}{\beta \cos\theta}, \tag{5}$$

where D, λ, k, and β are crystallite size, X-ray wavelength, Scherrer constant (=0.9), and full-width half maxima, respectively. Table 2 shows the average crystallite size for the synthesized complexes. No significant change in the crystallite size was observed when ZnO was calcined for 4 hours at 400°C which does not match with the previous report [37]. Moreover, the crystallite size of ZnO on AC is significantly smaller than that of ZnO alone. Though the ZnO/AC hydrothermal reaction was conducted for 24 hours long, the crystallite size is 16 nm. This implies that the environment for the crystallization of ZnO is not suitable when there is activated carbon in the solution.

No separate peak for nitrogen is observed. Figure 2 shows a minor peak shift after N-doping, moving towards lower values, indicating an increase in the interplanar space and a decrease in the lattice strain [36]. N-doping shows slight shrinking of the peak width and an increase in crystallinity as compared to pure ZnO. This represents that the crystal periodicity increased after N-doping, resulting in an increase in the crystallite size as shown in Table 2. These findings demonstrate that the addition of N to the ZnO lattice was successful. Moreover, the peak width for ZnO/AC

Table 2: Crystallite and particle sizes for synthesized complexes.

Complexes	Average crystallite size (nm) from XRD	Average particle size (nm) from TEM
(a) ZnO	23	27
(b) ZnO (400°C)	23	31
(c) N-ZnO	28	77
(d) ZnO/AC	16	60

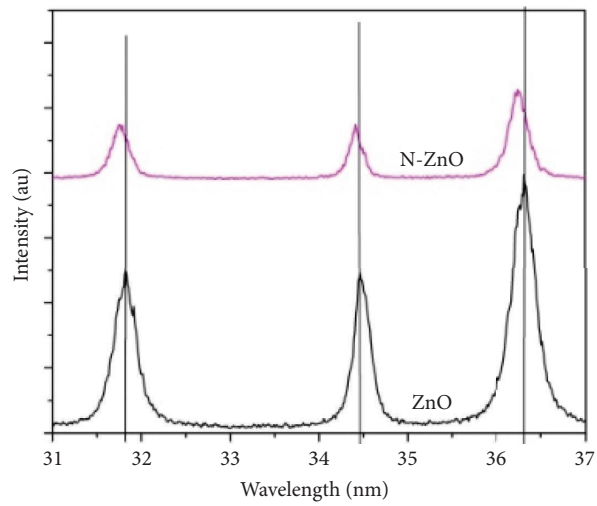

Figure 2: Peak shift of N-ZnO compared to ZnO.

is wide and its crystallinity is low as compared to other complexes.

3.1.2. SEM Analysis. Figures 3(a)–3(d) show the SEM images of ZnO, ZnO (calcined at 400°C), N-doped ZnO, and ZnO/AC nanocomposites, respectively. It is seen that all of the nanoparticles look like flowers and are loosely grouped into bush-like structures. Primary nanoparticles can form intricate assemblages known as aggregates or agglomerates in processes where particles originate by nucleation and growth. [38] These materials typically consist of spread of primary nanoscale (5–50 nm) aggregates that are chemically linked and typically range in size from 200 to 300 nm. The larger structures that are created by aggregates are known as agglomerates, and they are kept together by weaker forces such as electrostatics, van der Waals, solvation, or capillary actions [39]. From Figures 3(a) and 3(d), it is seen that there was no significant change in morphology between ZnO and N-doped ZnO. In ZnO (400°C), higher grain diameter is observed compared to ZnO. In ZnO/AC, the flower-like grains of ZnO are observed to be attached on top of the activated carbon. The morphology of the complexes was further studied by TEM.

3.1.3. EDS Analysis. The energy-dispersive X-ray spectroscopy (EDS) analysis determined the chemical composition of the samples as shown in Figure 4 and Table 3. The N-doped ZnO sample's EDS pattern reveals the presence of nitrogen (N), together with Zn and O, demonstrating the

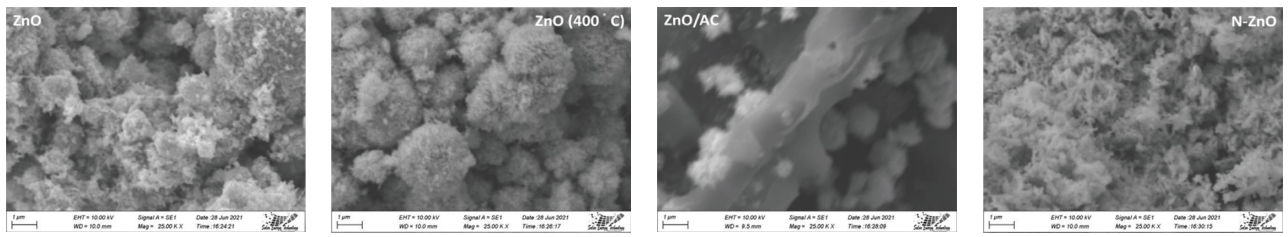

(a) (b) (c) (d)

Figure 3: The SEM images for all synthesized complexes of (a) ZnO, (b) ZnO (400°C), (c) ZnO/AC, and (d) N-ZnO.

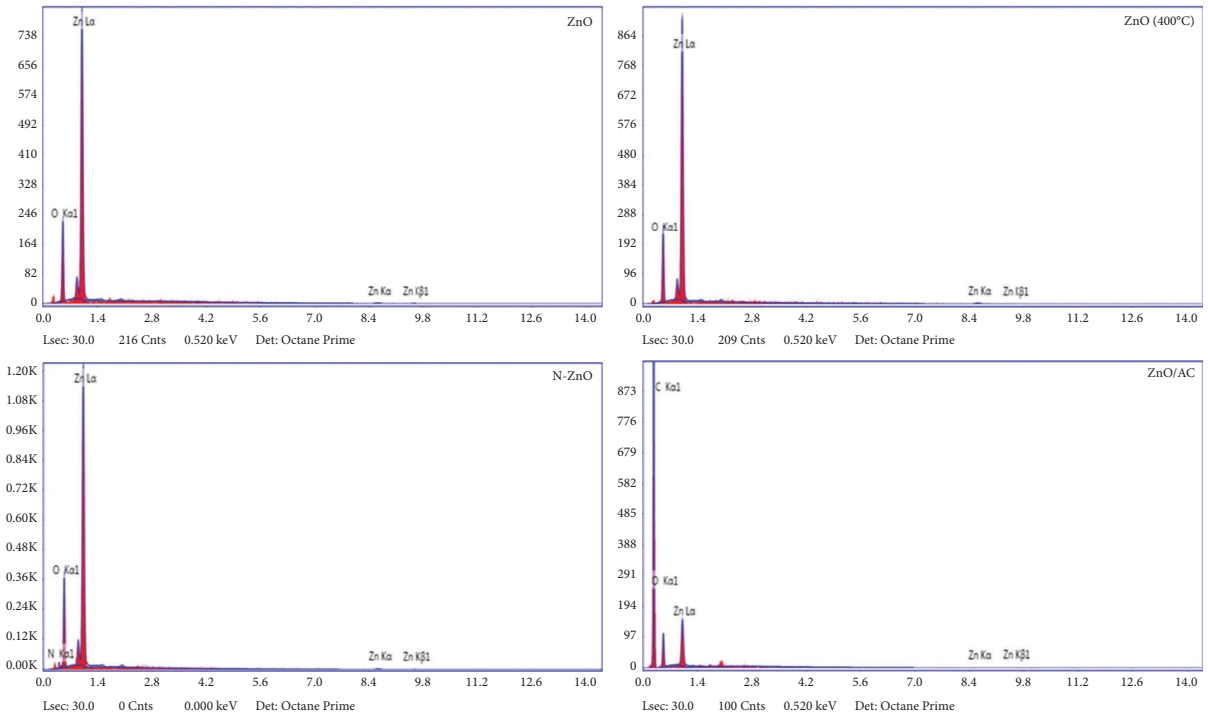

Figure 4: The traced elemental composition from EDS for all synthesized complexes.

Table 3: Atomic percentages for all synthesized complexes.

Complexes	Atomic % Zn	Atomic % O	Atomic % N	Atomic % C
ZnO	59.79	40.21		
ZnO (400°C)	60.97	39.03		
N-ZnO	53.71	40.06	6.22	
ZnO/AC	2.75	8.78		88.47

efficacy of nitrogen doping in the ZnO matrix. However, the EDS of ZnO/AC indicates that the percentage of ZnO on AC was low as shown in Figure 4.

3.1.4. FTIR Analysis. Due to the unique absorption of the Zn-O link in zinc oxide, all catalysts exhibit an absorption peak in the 400–600 cm^{-1} range [40, 41], shown in Figure 5. Also, the peak at 670 cm^{-1} corresponds to the vibrational energies of Zn-O, which confirms the formation of the ZnO phase [42]. The peak detected at ~1020 cm^{-1} is due to the C-H bending vibrations [43]. Those samples that display the transmittance band around 1600 cm^{-1} correspond to the bending vibrations of surface hydroxyl groups [44]. The peak at around 2360 cm^{-1} shows the presence of CO_2 [42]. The possible source of CO_2 is the atmosphere.

3.1.5. BET Analysis. The calculated total pore volume, BET surface area, and BJH pore size of ZnO/AC are 0.3257 cc/g, 558.14 m^2/g, and 2.3 nm, respectively. The mesoporous architecture and increased surface area are probably going to improve the adsorption performance [18].

3.1.6. UV-Visible Spectroscopy Analysis. Figure 6 shows the UV-visible spectra of the samples. The absorption peaks of pure ZnO appear at 366 nm which has not changed significantly due to calcination or incorporation with activated carbon. All the electromagnetic radiations from 200 to 800 nm are absorbed by AC, which is also confirmed by previous studies [35]. However, slight red shifting of the

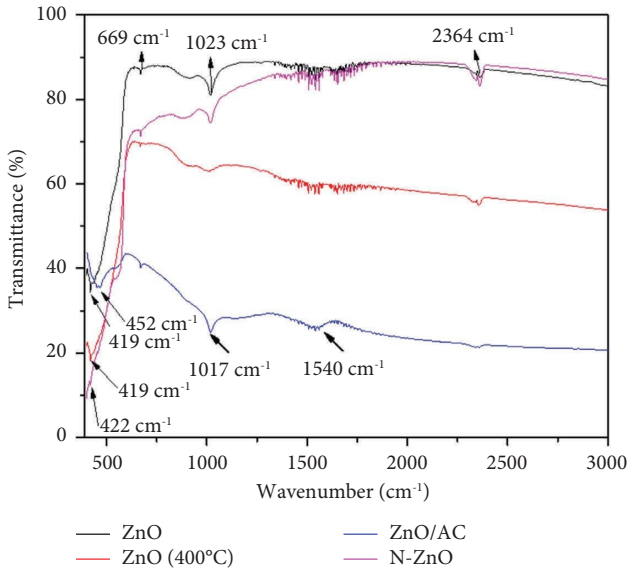

Figure 5: The FTIR for all synthesized complexes.

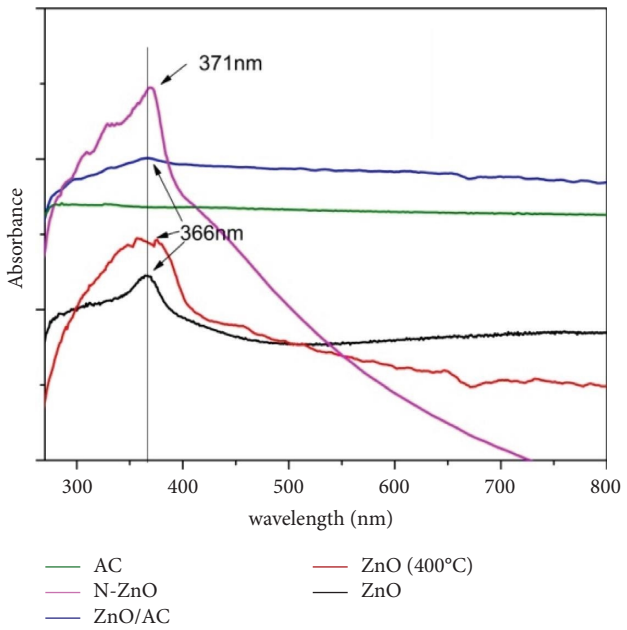

Figure 6: UV-vis spectra for all synthesized complexes.

absorption peak is observed due to N-doping, suggesting a decrease in the band gap compared to pure ZnO.

The band gap of the prepared samples has been estimated via the Tauc relation which is shown in the following equation:

$$(\alpha h\nu)^n = B(h\nu - \mathrm{Eg}), \tag{6}$$

where α is the absorption coefficient ($\alpha = 2.303$x A/t), A is absorbance, h is Planks' constant, ν is the frequency of the photon, B is the band tailing parameter, and Eg is the optical band gap. For direct and indirect transition, n is equal to 2 and ½, respectively. The direct optical band gap (Eg) of the synthesized ZnO nanostructures was ascertained from Tauc's plot by extrapolating the linear region of the $(\alpha h\nu)^2$ versus $(h\nu)$ curve [36], as shown in Figure 7.

From Tauc's plot (Figure 7), it is observed that the pure ZnO has a band gap of 2.8 eV. When compared to pure ZnO, ZnO (400°C), and N-ZnO, it showed a modest increase in the crystallite size, which led to a decrease in the band gap (2.7 eV) due to the quantum confinement effect [45]. However, the crystallite size decreased significantly in the case of ZnO/AC, and as a result, the band gap increased (4.1 eV) as shown in Table 4.

3.1.7. TEM Analysis. The TEM images in Figure 8 show that ZnO, ZnO (400°C), N-doped ZnO, and ZnO grown on AC nanoparticles are nonuniform and rod-shaped with curved ends projected out. Figure 8(a) shows many intermediate primary crystallites; they are joined together to form larger crystals [46]. The following action may take place in the autoclave as temperature and pressure rise under process conditions (150°C, 13 h):

$$\begin{aligned} \mathrm{Zn(OH)_4^{2-}} &= \mathrm{Zn^{2++}} + 4\mathrm{OH^-}\ \text{(dissolution)} \\ \mathrm{Zn^{2+}} + 2\mathrm{OH^-} &= \mathrm{ZnO} + \mathrm{H_2O}\ \text{(nucleation)} \end{aligned} \tag{7}$$

Fine ZnO nuclei spontaneously develop in the solution when the proportion of Zn^{2+} and OH^- is above saturation. The ZnO nuclei are combined together by interfacial energy, as they are unable to be combined with water solution. Also, it is possible to form crystals by growth in layers. The typical crystal habit and growth form or the preferential growing plane of ZnO is wurtzite under hydrothermal conditions. The growth plane was described by the "lowest-energy" theory [47]. Throughout the entire process, the rule is completely followed and single nanorods showed no signs of branching. The solution combination undergoes an ultrasonic pretreatment that causes nucleus development to be irregular and reduces aggregation.

Table 2 shows a comparison between crystallite sizes obtained from XRD and particle size from TEM. The nanorods have diameters between 20 and 80 nm and a length between 100 and 200 nm. The average diameters of ZnO and ZnO (400°C) are about 27 nm and 31 nm which are in better agreement with the size calculated by XRD. The particle size of ZnO at ZnO/AC is 60 nm which is very high compared to the crystallite size calculated by XRD. This is possibly because the hydrothermal reaction time was 24 hours for ZnO/AC which made the particle size large compared to the crystallite size. Also, the average particle size of N-ZnO is 77 nm.

Figures 9 and 10 show the selected area electron diffraction (SAED) pattern for all ZnO nanoparticle complexes. It shows that the particles are well crystallized. The hexagonal wurtzite structure of ZnO nanoparticles is further demonstrated by the matching of the diffraction rings on the (SAED) image with the peaks in the XRD pattern as shown in Figure 1 [48].

3.2. Removal of MNZ by ZnO Nanoparticles. At photocatalytic doses of 0.9 g·L^{-1} and MNZ contents of 80 mg·L^{-1}, 83%, 89%, 66%, and 99% MNZ removal was observed in

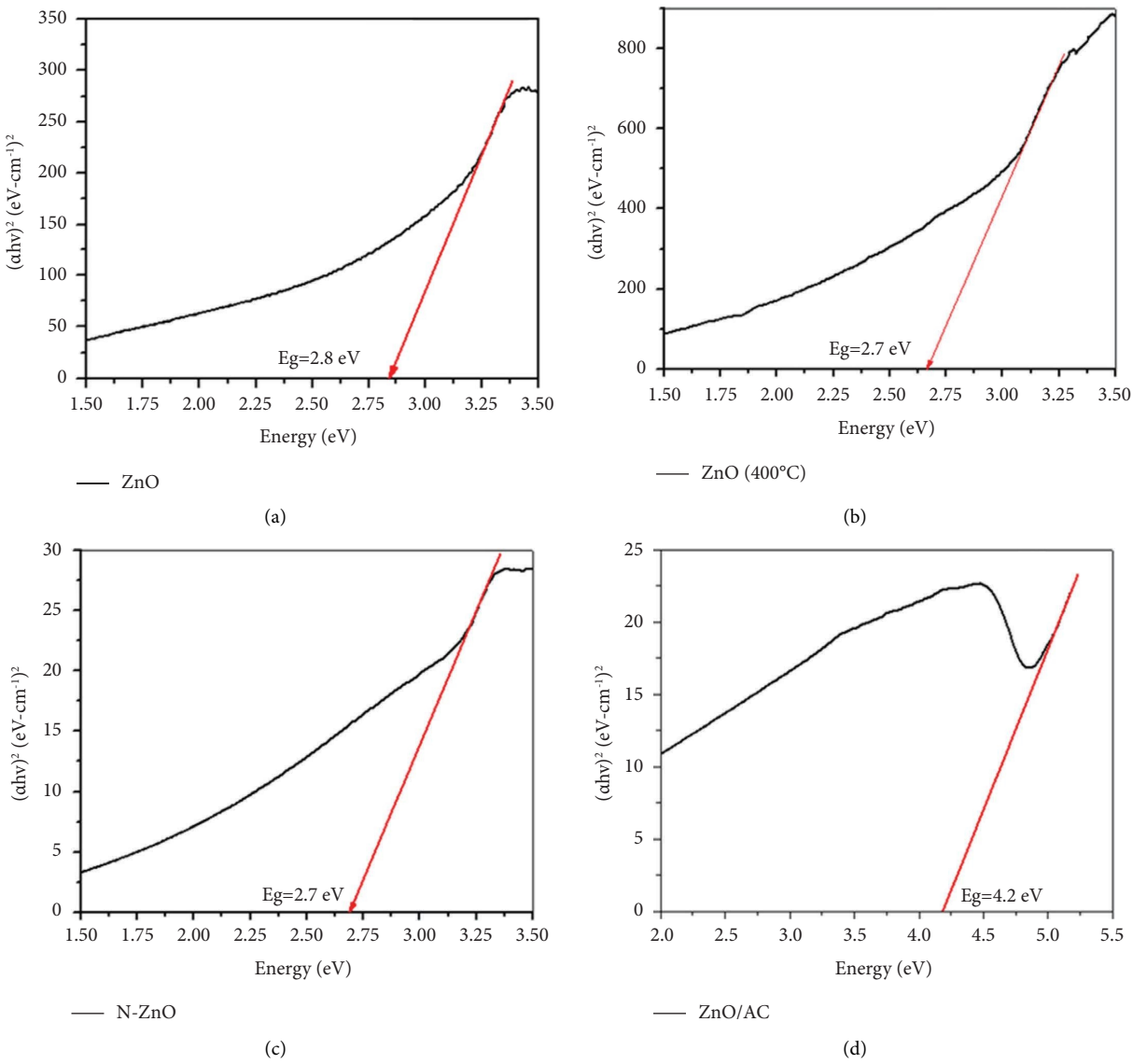

Figure 7: Direct optical band gap for (a) ZnO, (b) ZnO calcined at 400°C, (c) N-doped ZnO, and (d) ZnO/AC.

Table 4: Optical band gaps.

Complexes	Direct band gap (eV)
ZnO	2.8
ZnO (400°C)	2.7
N-ZnO	2.7
ZnO/AC	4.1

ZnO, ZnO(400°C), N-ZnO, and ZnO/AC systems, respectively, in 300 minutes (Figure 11). At lesser MNZ levels, such as 10, 20, 30, 40, and 50 mg·L^{-1}, a similar MNZ elimination pattern was seen. According to the current investigation, the ZnO/AC system generated full MNZ elimination at a faster rate. This is due to the synergistic action of MNZ adsorbed on photocatalytic composites embedded with ZnO/AC, which combines adsorption with photocatalytic disintegration using hydroxyl radicals. MNZ adsorption on ZnO/AC was indeed the maximum and the fastest when compared to MNZ elimination by adsorption utilizing all others shown in Figure 11. Also, the degradation rate constant is compared for all the synthesized complexes in Figure 12. Since the rate constant is higher for ZnO/AC, the effect of catalytic dose, pH, and degradation intermediates were studied by using this.

Figure 13 shows the adsorption in the dark when AC was used alone compared to ZnO/AC. It was found that AC decreased 60% of MNZ in the solution almost immediately. Since ZnO is a photocatalyst, ZnO along with AC worked better for eliminating MNZ completely. The rapid fluctuation indicates that desorption also took place.

3.2.1. Catalyst Dosage Effect. Figure 14 shows the effect of catalyst doses from 0.3 g/L to 1.1 g/L for adsorption and photodegradation of ZnO/AC on MNZ. The solution was stirred in the dark for 30 minutes for the adsorption to happen, and then the UV light was irradiated on the

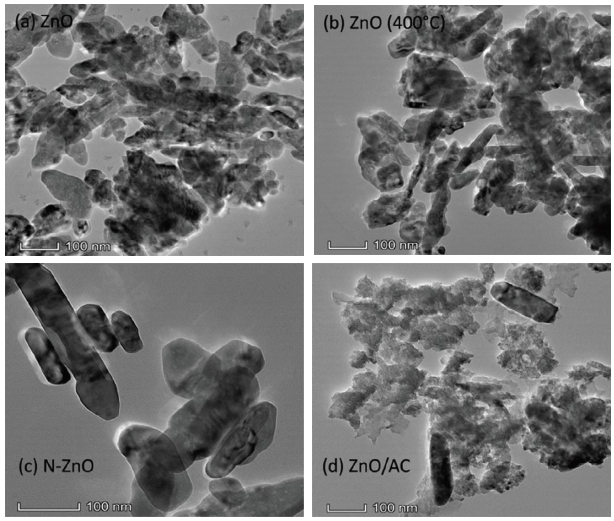

Figure 8: TEM images for all synthesized complexes of (a) ZnO, (b) ZnO (400°C), (c) N-ZnO, and (d) ZnO/AC.

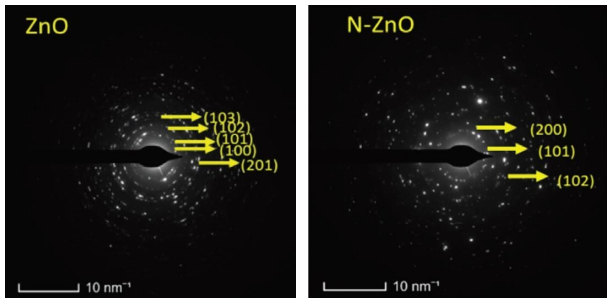

Figure 9: SAED for ZnO and N-ZnO nanocomposites.

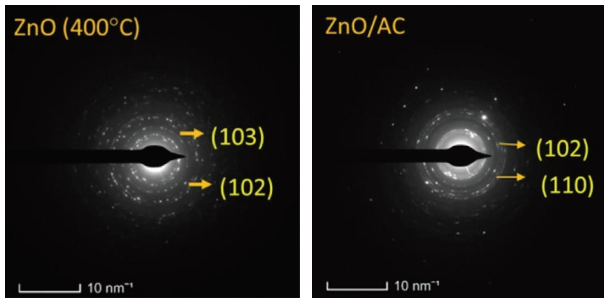

Figure 10: SAED for ZnO (400°C) and ZnO/AC nanocomposites.

solution. In the dark regions, the more the dose, the greater is the adsorption. 0.9 g/L is the optimum dose where degradation was the maximum. When the photocatalytic doses increased, the active site generated was larger which contributed to an increase in the degradation rate. However, when the dose is increased, UV light is blocked or scattered by the suspended photocatalysts.

3.2.2. Effect of pH on Degradation. At pH of less than 4, MNZ is called protonated, and at pH greater than 12, it is called anionic [49]. The photocatalytic degradation of MNZ over ZnO/AC at different pH values is shown in Figure 15. It

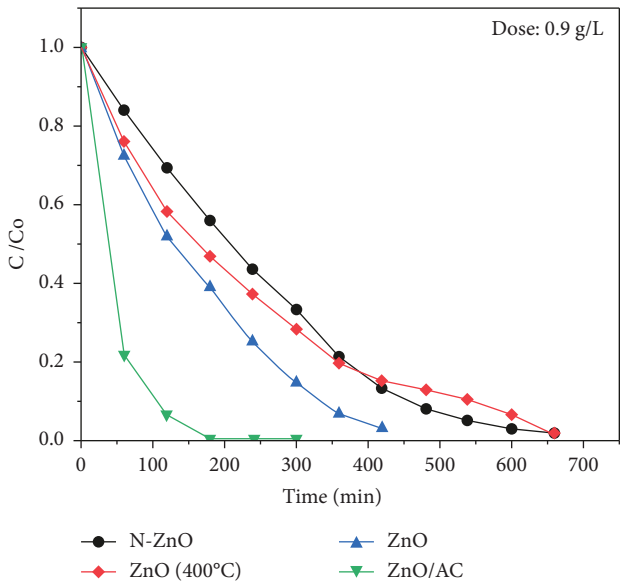

Figure 11: MNZ removal pattern by ZnO, ZnO (400°C), N-ZnO, and ZnO/AC.

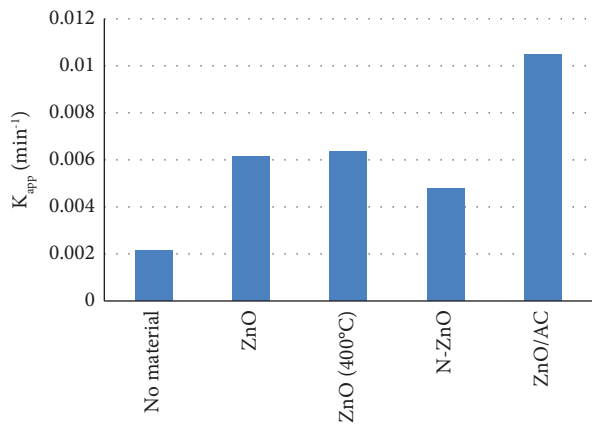

Figure 12: The apparent rate constants for ZnO, ZnO (400°C), N-ZnO, and ZnO/AC (MNZ 80 mg/L, catalytic dose 0.9 g/L, and pH 9).

is found that the rate of photodegradation is stable over pH from 5 to 9, but K_{app} is low at low pH due to its electrostatic interaction with the catalyst. However, MNZ disappears almost immediately after it reaches a high pH value. So, pH = 9 is considered to be the optimal pH value. Very similar findings were also obtained by other researchers [49].

3.2.3. Intermediates' Identification. When UV light is absorbed by a ZnO photocatalyst, negative electron and positive hole pairs are thought to form. While ZnO's positive holes break up water molecules to form hydrogen ions and hydroxyl radicals, ZnO's negative electrons interact with oxygen molecules to form superoxide radicals. Superoxide and hydroxyl radicals are powerful oxidants of organic materials. Consequently, the photocatalysis of MNZ to

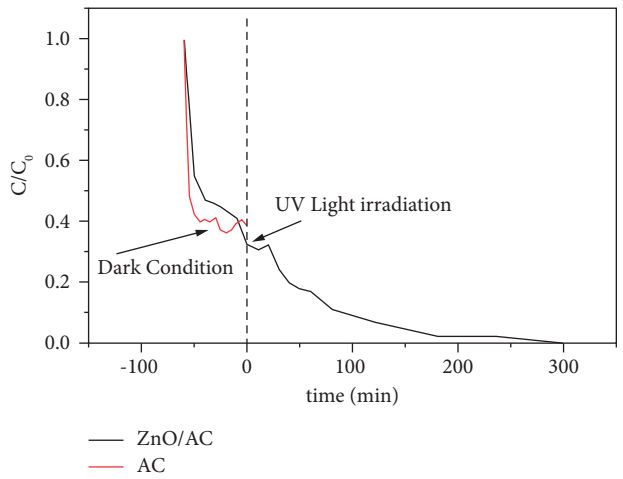

Figure 13: UV visible spectroscopy graph for MNZ degradation by ZnO/AC and AC.

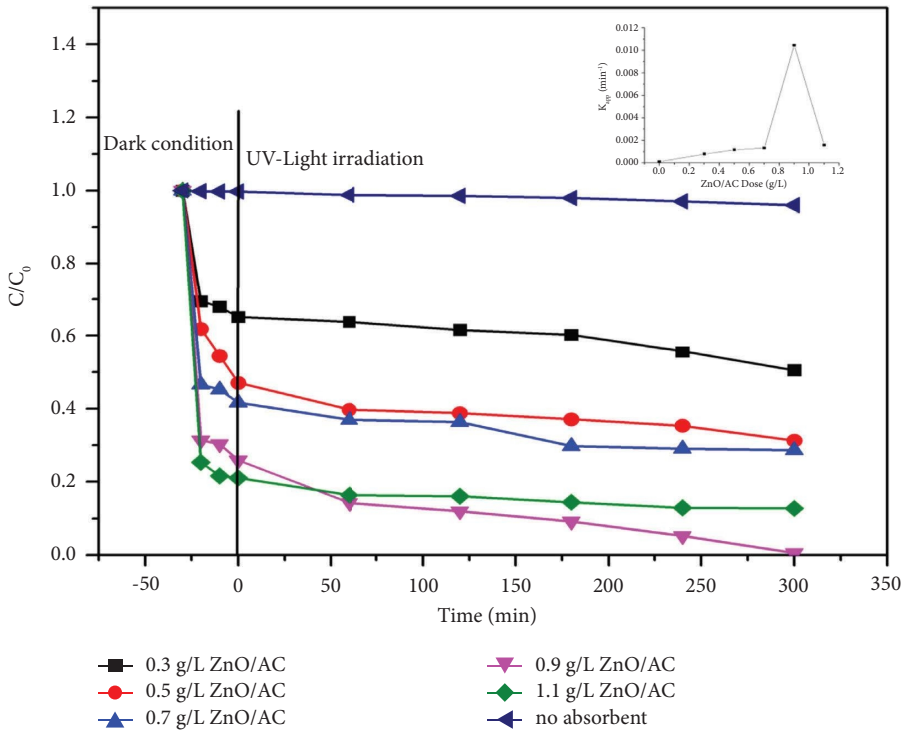

Figure 14: The effect of catalyst dose of ZnO/AC.

smaller byproducts is caused by the incidence of UV light at the catalyzed reaction.

The intermediates were discovered using LC-MS and GC-MS after metronidazole was removed using ZnO/AC. SHIMADZU LC-MS 8050 together with LabSolution software was used to perform LC-MS. Also, a gas chromatography (model no 8890) (Agilent Technologies, USA) system coupled with a mass spectroscopy (5977B) detector along with mass hunter analytical software was used to identify the intermediates. The results of LC-MS and GC-MS analysis were combined together to find a pathway of degradation, as shown in Figure 16. The oxidation of the methyl group may result in the formation of an intermediate of m/z 126, the loss of nitro groups, and water elimination. The m/z 172 seems to be the rearrangement of MNZ, and m/z 158 is also the cleavage form of m/z 172. There were also other intermediates with reduced molecular weights. Those were created when metronidazole was broken down, and they were then transformed into CO_2, NO_2, H_2O, and NH_3. Figure 16 shows a potential mechanism for disintegration.

3.2.4. Stability and Reusability of ZnO/AC. Due to its vast surface area and numerous active sites, ZnO/AC is stable and recyclable. These sites are where molecules are adsorbed and photogenerated charge carriers react to form hydroxyl

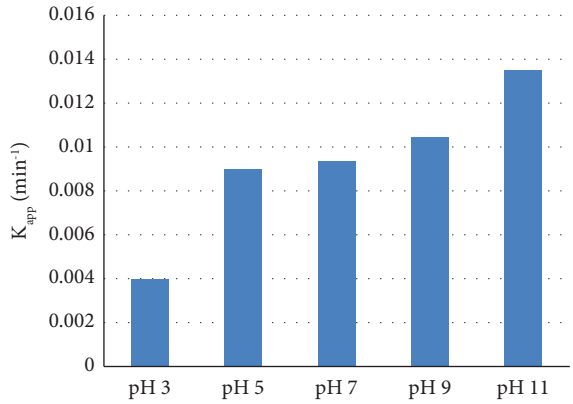

Figure 15: The apparent rate constants for degradation of MNZ with ZnO/AC catalyst at different pH values (MNZ 80 mg/L and catalytic dose 0.9 g/L).

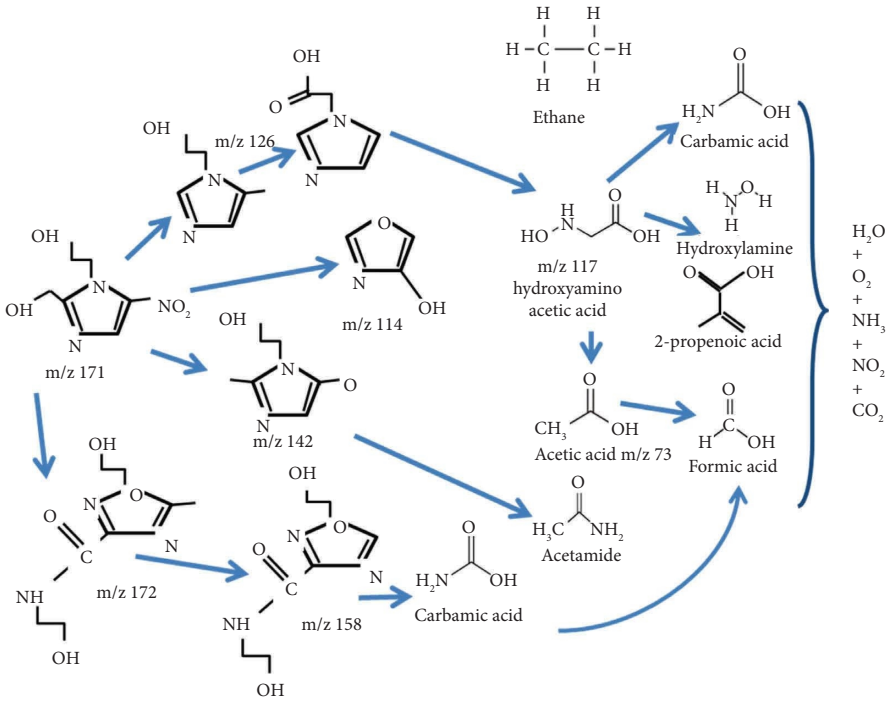

Figure 16: Proposed degradation intermediates of MNZ by ZnO/AC photocatalyst under UV irradiation.

and oxide radicals. The reusability of the composite was investigated in three photocatalytic tests, each lasting for 180 minutes. At the end of each cycle, the samples were tested to determine the MNZ content. Filtering these particles with Whatman filter paper was quick, but the removal efficiency was poor. This technique of filtering removes all traces of ZnO from the nanopowder ZnO/AC(W), as shown in Figure 17.

The test was therefore started from scratch. Although it took longer, 0.45 μm nylon 6,6 membranes were utilized this time to obtain the particles. Figure 18 shows how the ZnO/AC composites exhibited high photocatalytic performance throughout the duration of three cycles of usage and regeneration while maintaining their stability. After the first, second, and third cycles in the presence of ZnO/AC, the removal of 80 mg/L MNZ was greater than 99%, 98%, and 97%, respectively, after 300 minutes. This pattern was attributed to the gradual removal of ZnO from the AC surface during cleaning. The elimination capability of the composite material was also shown to be unaffected after three cycles by

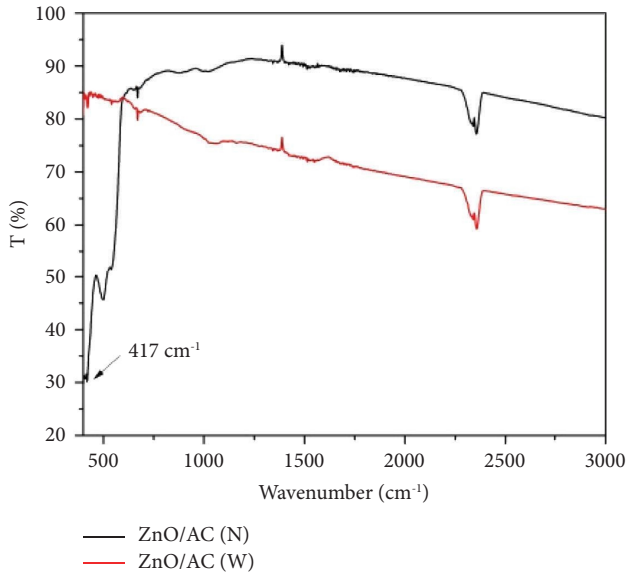

Figure 17: FTIR of the nanopowder after filtering with Whatman filter paper (ZnO/AC(W)) and nylon membrane filter (ZnO/AC(N)).

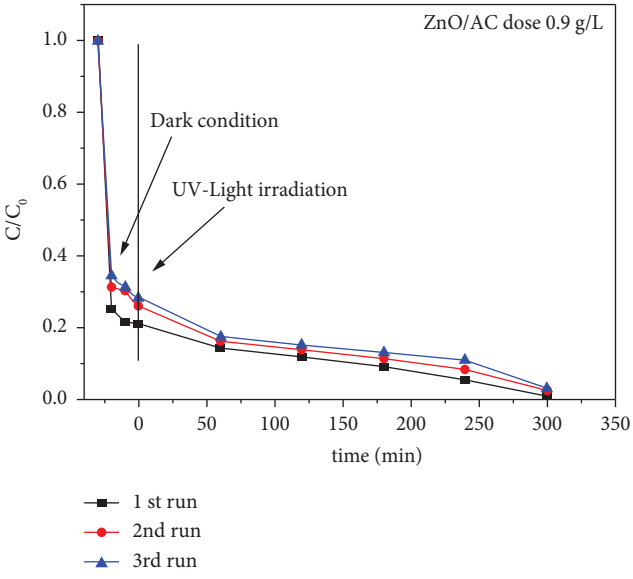

Figure 18: Reusability test by ZnO/AC.

the FTIR patterns shown in Figure 17 ZnO/AC(N). This established the suitability of the ZnO/AC composite material for application in industrial design and production for the eradication of MNZ.

4. Conclusion

In this study, ZnO, nitrogen-doped ZnO nanoparticles, and AC impregnated with ZnO (ZnO/AC) nanocomposites were synthesized by the hydrothermal method and applied for photocatalytic removal of metronidazole (MNZ) antibiotic from aqueous solutions under UV light. The removal efficiencies were compared in a way of how fast they can degrade MNZ from water. It takes around 660 minutes for N-ZnO and ZnO (400°C) to separately disintegrate MNZ. After calcination, the band gap of ZnO is lowered, but probably, the aggregation of ZnO (400°C) made it difficult to incorporate it with water. However, ZnO/AC was the fastest in degrading metronidazole and 60% of MNZ can be adsorbed by AC alone. The highly porous AC captures MNZ molecules, but MNZ is not degraded by AC, and there is a chance of desorption. So, for splitting MNZ under UV light, ZnO was incorporated with AC. ZnO produces superoxide and hydroxyl radicals in an aqueous medium under UV light that oxidizes MNZ, which in turn produces smaller byproducts. The trace of these residues in water will have various consequences and can pose a health hazard for humans and animals. These ZnO composites are stable in a wide range of pH and reusable for various cycles. The reusability technique was examined keenly and explained. Reusability testing was shown to be successful when 0.45 m nylon 6,6 membranes were employed for filtering. The result indicates that ZnO/AC can be a very promising nanocomposite over ZnO and N-ZnO for the degradation of MNZ from waste water.

Data Availability

The data used to support the findings of the study are available from the corresponding author upon request.

Conflicts of Interest

The authors declare that they have no conflicts of interest.

Acknowledgments

This research was accomplished by the financial support of the Ministry of Science and Technology, Bangladesh, and the University Grants Commission of Bangladesh. The authors are grateful to Md. Abdul Gafur, PP&PDC, Bangladesh Council of Scientific and Industrial Research (BCSIR), Dhaka, Bangladesh, and M. S. Bashar, IFRD, BCSIR, for providing us the contributions in characterization. In addition, the authors would like to acknowledge the Atomic Energy Commission of Bangladesh and the Department of Chemical Engineering at the Bangladesh University of Engineering & Technology in Dhaka, Bangladesh, for their characterization support.

References

[1] O. E. Pemra Nesil, "Foodborne and infant botulism linkage with the gut microbiome ' s impact on the immune system and mental function," *Journal of Experimental and Basic Medical Sciences*, vol. 2, no. 3, 2022.

[2] M. Cherington, "Botulism: update and review," *Seminars in Neurology*, vol. 24, no. 02, pp. 155–163, 2004.

[3] Z. A. Bhutta, "Current concepts in the diagnosis and treatment of typhoid fever," *British Medical Journal*, vol. 333, no. 7558, pp. 78–82, 2006.

[4] S. H. E. Kaufmann, "Tuberculosis: back on the immunologists' agenda," *Immunity*, vol. 24, no. 4, pp. 351–357, 2006.

[5] M. A. Kohanski, D. J. Dwyer, and J. J. Collins, "How antibiotics kill bacteria: from targets to networks," *Nature Reviews Microbiology*, vol. 8, no. 6, pp. 423–435, 2010.

[6] S. S. Boxi and S. Paria, "Effect of silver doping on TiO2, CdS, and ZnS nanoparticles for the photocatalytic degradation of metronidazole under visible light," *RSC Advances*, vol. 4, no. 71, pp. 37752–37760, 2014.

[7] D. G. J. Larsson and C. F. Flach, "Antibiotic resistance in the environment," *Nature Reviews Microbiology*, vol. 20, no. 5, pp. 257–269, 2022.

[8] S. Yao, J. Ye, Q. Yang et al., "Occurrence and removal of antibiotics, antibiotic resistance genes, and bacterial communities in hospital wastewater," *Environmental Science & Pollution Research*, vol. 28, no. 40, pp. 57321–57333, 2021.

[9] J. L. Martinez, "Environmental pollution by antibiotics and by antibiotic resistance determinants," *Environmental Pollution*, vol. 157, no. 11, pp. 2893–2902, 2009.

[10] U. Szymańska, M. Wiergowski, I. Sołtyszewski, J. Kuzemko, G. Wiergowska, and M. K. Woźniak, "Presence of antibiotics in the aquatic environment in Europe and their analytical monitoring: recent trends and perspectives," *Microchemical Journal*, vol. 147, pp. 729–740, 2018.

[11] K. G. Karthikeyan and M. T. Meyer, "Occurrence of antibiotics in wastewater treatment facilities in Wisconsin, USA," *Science of the Total Environment*, vol. 361, no. 1–3, pp. 196–207, 2006.

[12] L. F. Angeles, S. Islam, J. Aldstadt et al., "Retrospective suspect screening reveals previously ignored antibiotics, antifungal compounds, and metabolites in Bangladesh surface waters," *Science of the Total Environment*, vol. 712, Article ID 136285, 2020.

[13] F. Hernández, N. Calısto-Ulloa, C. Gómez-Fuentes et al., "Occurrence of antibiotics and bacterial resistance in wastewater and sea water from the Antarctic," *Journal of Hazardous Materials*, vol. 363, pp. 447–456, 2018.

[14] S. Liu, G. Zhao, H. Zhao, G. Zhai, J. Chen, and H. Zhao, "Antibiotics in a general population: relations with gender, body mass index (BMI) and age and their human health risks," *Science of the Total Environment*, vol. 599-600, no. 600, pp. 298–304, 2017.

[15] H. Sørum and M. Sunde, "Resistance to antibiotics in the normal flora of animals," *Veterinary Research*, vol. 32, no. 3-4, pp. 227–241, 2001.

[16] A. Mann, K. Nehra, J. S. Rana, and T. Dahiya, "Antibiotic resistance in agriculture: perspectives on upcoming strategies to overcome upsurge in resistance," *Current Research in Microbial Sciences*, vol. 2, Article ID 100030, 2020.

[17] D. G. J. Larsson, "Antibiotics in the environment," *Upsala Journal of Medical Sciences*, vol. 119, no. 2, pp. 108–112, 2014.

[18] M. Farzadkia, E. Bazrafshan, A. Esrafili, J. K. Yang, and M. Shirzad-Siboni, "Photocatalytic degradation of Metronidazole with illuminated TiO2 nanoparticles," *Journal of Environmental Health Science and Engineering*, vol. 13, no. 1, pp. 35–38, 2015.

[19] M. L. Tran, C. H. Nguyen, C. C. Fu, and R. S. Juang, "Hybridizing Ag-Doped ZnO nanoparticles with graphite as potential photocatalysts for enhanced removal of metronidazole antibiotic from water," *Journal of Environmental Management*, vol. 252, Article ID 109611, 2019.

[20] G. Prados-Joya, M. Sánchez-Polo, J. Rivera-Utrilla, and M. Ferro-garcía, "Photodegradation of the antibiotics nitroimidazoles in aqueous solution by ultraviolet radiation," *Water Research*, vol. 45, no. 1, pp. 393–403, 2011.

[21] W. Cheng, M. Yang, Y. Xie, Z. Fang, J. Nan, and P. E. Tsang, "Electrochemical degradation of the antibiotic metronidazole in aqueous solution by the Ti/SnO 2-Sb-Ce anode," *Environmental Technology*, vol. 34, no. 21, pp. 2977–2987, 2013.

[22] N. Nasseh, F. S. Arghavan, S. Rodriguez-Couto, A. Hossein Panahi, M. Esmati, and T. J. A-Musawi, "Preparation of activated carbon@ZnO composite and its application as a novel catalyst in catalytic ozonation process for metronidazole degradation," *Advanced Powder Technology*, vol. 31, no. 2, pp. 875–885, 2020.

[23] H. B. Ammar, "Sono-Fenton process for metronidazole degradation in aqueous solution: effect of acoustic cavitation and peroxydisulfate anion," *Ultrasonics Sonochemistry*, vol. 33, pp. 164–169, 2016.

[24] M. L. Tran, C. C. Fu, and R. S. Juang, "Removal of metronidazole by TiO2 and ZnO photocatalysis: a comprehensive comparison of process optimization and transformation products," *Environmental Science & Pollution Research*, vol. 25, no. 28, pp. 28285–28295, 2018.

[25] A. N. Alibeigi, N. Javid, M. Amiri Gharaghani, Z. Honarmandrad, and F. Parsaie, "Synthesis, characteristics, and photocatalytic activity of zinc oxide nanoparticles stabilized on the stone surface for degradation of metronidazole from aqueous solution," *Environmental Health Engineering and Management*, vol. 8, no. 1, pp. 55–63, 2021.

[26] M. G. Batterjee, A. Nabi, M. R. Kamli, K. A. Alzahrani, E. Y. Danish, and M. A. Malik, "Green hydrothermal synthesis of zinc oxide nanoparticles for UV-Light-Induced photocatalytic degradation of ciprofloxacin antibiotic in an aqueous environment," *Catalysts*, vol. 12, no. 11, pp. 1347–1417, 2022.

[27] H. A. Dessouki, G. El-Sayed, H. Jahin, and S. Ibrahiem, "Photocatalytic degradation of metronidazole in aqueous solutions by copper oxide nanoparticles," *Journal of Basic and Environmental Sciences*, vol. 1, pp. 102–110, 2014.

[28] S. Ahmadzadeh and M. Dolatabadi, "Electrochemical treatment of pharmaceutical wastewater through electrosynthesis of iron hydroxides for practical removal of metronidazole," *Chemosphere*, vol. 212, pp. 533–539, 2018.

[29] N. Nasseh, B. Barikbin, L. Taghavi, and M. A. Nasseri, "Adsorption of metronidazole antibiotic using a new magnetic nanocomposite from simulated wastewater (isotherm, kinetic and thermodynamic studies)," *Composites Part B: Engineering*, vol. 159, pp. 146–156, 2019.

[30] E. Prabakaran and K. Pillay, "Synthesis of N-doped ZnO nanoparticles with cabbage morphology as a catalyst for the efficient photocatalytic degradation of methylene blue under UV and visible light," *RSC Advances*, vol. 9, no. 13, pp. 7509–7535, 2019.

[31] J. Akhtar, M. B. Tahir, M. Sagir, and H. S. Bamufleh, "Improved photocatalytic performance of Gd and Nd co-doped ZnO nanorods for the degradation of methylene blue," *Ceramics International*, vol. 46, no. 8, pp. 11955–11961, 2020.

[32] M. Sivachidambaram, J. J. Vijaya, L. J. Kennedy et al., "Preparation and characterization of activated carbon derived from the Borassus flabellifer flower as an electrode material for supercapacitor applications," *New Journal of Chemistry*, vol. 41, 2017.

[33] T. Yue, B. Shen, and P. Gao, "Carbon material/MnO2 as conductive skeleton for supercapacitor electrode material: a review," *Renewable and Sustainable Energy Reviews*, vol. 158, Article ID 112131, 2022.

[34] S. Begum and M. Ahmaruzzaman, "Biogenic synthesis of SnO 2/activated carbon nanocomposite and its application as

photocatalyst in the degradation of naproxen," *Applied Surface Science*, vol. 449, pp. 780–789, 2018.

[35] V. H. Tran Thi and B. K. Lee, "Great improvement on tetracycline removal using ZnO rod-activated carbon fiber composite prepared with a facile microwave method," *Journal of Hazardous Materials*, vol. 324, pp. 329–339, 2017.

[36] A. M. Manoj, L. R. Viannie, C. K. Subramaniam, N. A. N. Raj, and G. Manivasagam, "Single-step hydrothermal synthesis of nitrogen-doped ZnO nanostructures and an insight into its electrochemical properties," *Journal of Materials Research*, vol. 36, no. 2, pp. 350–360, 2021.

[37] S. Li, S. J. Silvers, and M. Samy El-Shall, "Preparation, characterization and optical properties of zinc oxide nanoparticles," *MRS Proceedings*, vol. 452, pp. 389–394, 1996.

[38] M. L. Eggersdorfer and S. E. Pratsinis, "Agglomerates and aggregates of nanoparticles made in the gas phase," *Advanced Powder Technology*, vol. 25, no. 1, pp. 71–90, 2014.

[39] S. C. Endres, L. C. Ciacchi, and L. Mädler, "A review of contact force models between nanoparticles in agglomerates, aggregates, and films," *Journal of Aerosol Science*, vol. 153, Article ID 105719, 2021.

[40] N. Goswami and D. K. Sharma, "Structural and optical properties of unannealed and annealed ZnO nanoparticles prepared by a chemical precipitation technique," *Physica E: Low-Dimensional Systems and Nanostructures*, vol. 42, no. 5, pp. 1675–1682, 2010.

[41] A. B. Lavand and Y. S. Malghe, "Synthesis, characterization and visible light photocatalytic activity of nitrogen-doped zinc oxide nanospheres," *Journal of Asian Ceramic Societies*, vol. 3, no. 3, pp. 305–310, 2015.

[42] M. S. Jabir, T. M. Rashid, U. M. Nayef et al., "Inhibition of Staphylococcus aureus α-hemolysin production using nanocurcumin capped Au@ZnO nanocomposite," *Bioinorganic Chemistry and Applications*, vol. 2022, Article ID 2663812, 18 pages, 2022.

[43] S. M. El-khouly, G. M. Mohamed, N. A. Fathy, and G. A. Fagal, "Effect of nanosized CeO 2 or ZnO loading on adsorption and catalytic properties of activated carbon," *Adsorption Science and Technology*, vol. 35, no. 9-10, pp. 774–788, 2017.

[44] F. Ghribi, M. Sehailia, L. Aoudjit et al., "Journal of Photochemistry & Photobiology A: chemistry Solar-light promoted photodegradation of metronidazole over ZnO-ZnAl 2 O 4 heterojunction derived from 2D-layered double hydroxide structure," *Journal of Photochemistry and Photobiology A: Chemistry*, vol. 397, Article ID 112510, 2020.

[45] S. Sun, X. Chang, X. Li, and Z. Li, "Synthesis of N-doped ZnO nanoparticles with improved photocatalytical activity," *Ceramics International*, vol. 39, no. 5, pp. 5197–5203, 2013.

[46] J. T. Sampanthar and H. C. Zeng, "Arresting butterfly-like intermediate nanocrystals of β-Co(OH)2 via ethylenediamine-mediated synthesis," *Journal of the American Chemical Society*, vol. 124, no. 23, pp. 6668–6675, 2002.

[47] L. Guo, Y. L. Ji, H. Xu, P. Simon, and Z. Wu, "Regularly shaped, single-crystalline ZnO nanorods with wurtzite structure," *Journal of the American Chemical Society*, vol. 124, no. 50, pp. 14864-14865, 2002.

[48] A. J. Ahamed and P. Vijaya Kumar, "Synthesis and characterization of ZnO nanoparticles by co-precipitation method at room temperature," *Journal of Chemical and Pharmaceutical Research*, vol. 8, no. 5, pp. 624–628, 2016.

[49] D. H. Carrales-Alvarado, R. Ocampo-Pérez, R. Leyva-Ramos, and J. Rivera-Utrilla, "Removal of the antibiotic metronidazole by adsorption on various carbon materials from aqueous phase," *Journal of Colloid and Interface Science*, vol. 436, pp. 276–285, 2014.